Performance Comparison Between Boost-based Closed-loop and Open-loop Maximum Power Point Tracking Techniques of Photovoltaic in Islanded Microgrid Environment

Lindemberg R. de Lima * **Luana C. S. Soares** **
Pedro A. de Alcântara ** **Camila M. V. Barros** ***
Luciano S. Barros ***

* *Graduate Program in Computational Mathematical Modelling, Federal University of Paraíba, PB, (e-mail: lindemberg.roberto@academico.ufpb.br)*
** *Electrical Engineering Graduate Program, Federal University of Paraíba, PB, (e-mails: luana.soares@cear.ufpb.br, pedro.alcantra@cear.ufpb.br).*
*** *Computer Systems Department, Informatic Center, Federal University of Paraíba,PB, (e-mails: camila.barros@ci.ufpb.br, lsalesbarros@ci.ufpb.br)*

Abstract:
In microgrids based on photovoltaic/battery generation, uncertainties during islanded operation can cause voltage and frequency fluctuations, making the control systems involved in the microgrid more difficult to action. From the photovoltaic maximum power point tracking (MPPT) point of view, to reduce the effects of uncertainties it is necessary to use a more robust method that guarantees correct supplying. In this paper, a comparison between two MPPTs based on the conventional Perturb & Observe algorithm is proposed, in the first one MPPT directly returns the duty-cycle for the DC-DC boost converter, being denominated of open-loop, and in the second one, the MPPT output voltage signal passes through internal cascaded proportional-integral loops before being converted in duty-cyle signal, being denominated of closed-loop. The objective is to evaluate the robustness provided by the closed-loop method, especially during the islanded operation. Both algorithms were simulated in MATLAB/Simulink with a 1,725W photovoltaic array (RISEM RMS 72-6-345P). The comparison analysis is based on the power quality delivered to the load through the observation of total harmonic distortion (THD), ripple level, settling time, and steady-state error. Results suggest that the closed-loop method provides a better and more reliable MPPT.

Keywords: microgrid, battery, photovoltaic, maximum power point tracking, islanding.

1. INTRODUCTION

The growing demand for renewable energy sources in recent decades has led to the emergence of microgrids (MG) as decentralized sources of energy connected to the utility's main grid as defined by Karimi et al. (2017). One of the most important renewable energy sources is photovoltaics (PV), whose capture has been made possible by the intensive use of semiconductors and the advancement of power electronics converter technology.

The efficient use of the energy generated from PV requires the study and improvement of techniques that allow the extraction of maximum power. It is commonly carried out through algorithms that track the maximum power point (MPP), being Perturb & Observe (P&O) the most reported method, described in Esram and Chapman (2007).

The P&O has the advantages of being efficient, easy computational implementation, and adaptation to different conditions of temperature and irradiance, but it has disadvantages oscillations around the MPP and the fact that it may fail in face of rapid variations in environment conditions (Esram and Chapman, 2007).

Many techniques have already been implemented and published, to provide more robustness for MPPT in face of environmental variations, including variable step size of P&O (Jiandong et al., 2018), incremental conductance method (Kim et al., 2020), ripple correlation control (Deshpande and Patil, 2016), fuzzy logic method (Rai and Rahi, 2022), neural network (Harrag et al., 2019) and current or voltage-oriented control technique (Mahmood et al., 2015), and (Raiker et al., 2021).

However, it is also important to investigate the P&O performance when PV units are in an islanded MG paradigm since the busbar AC terminal voltage can suffer significant fluctuations in magnitude and frequency due to unbalance between generation and load (Nguyen et al., 2019).

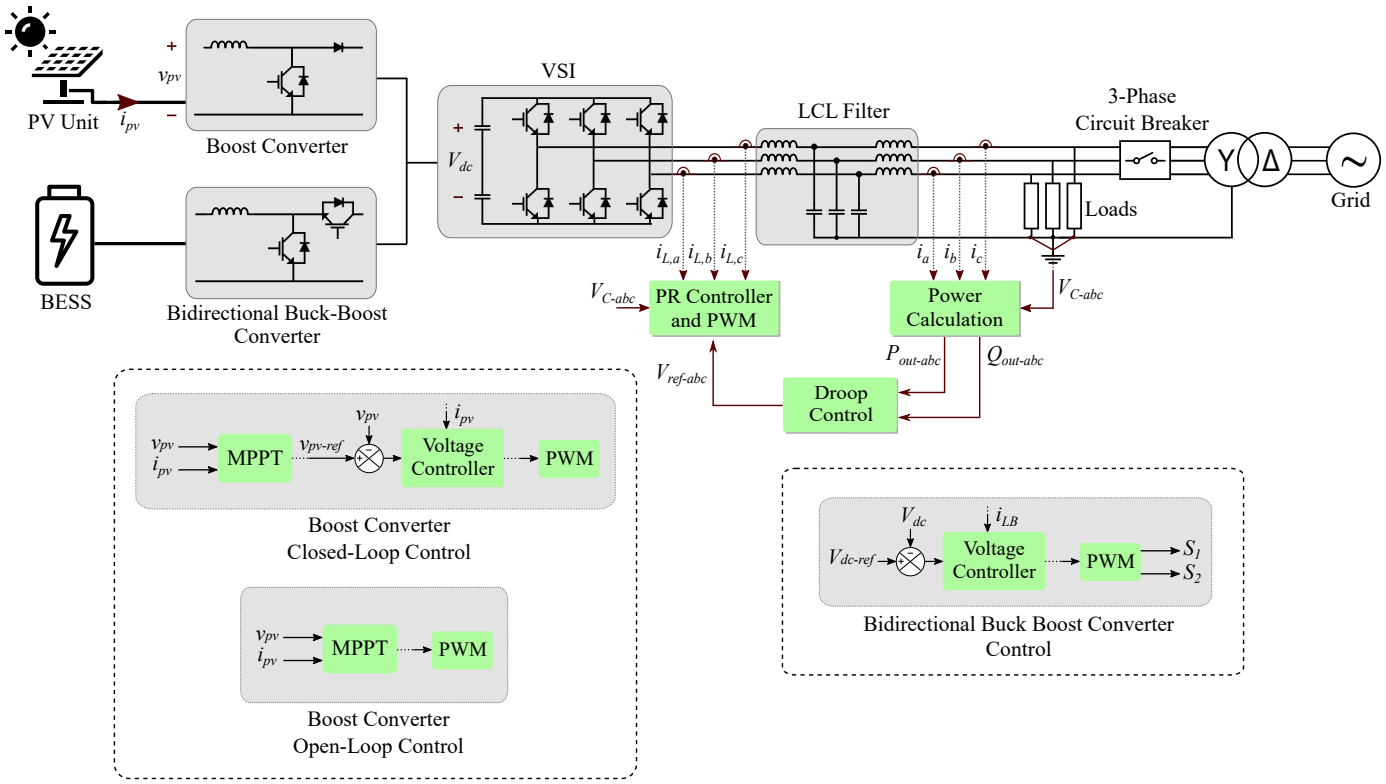

Figure 1. Microgrid architecture studied in this paper.

These fluctuations can compromise the performance of the P&O algorithm, causing unwanted uncertainties in the PV power generation. As a result, battery malfunction and loss of DC bus control can occur. Therefore, a robust MPPT is required to withstand fluctuations in the islanded MG.

In this paper, to test and improve the performance of the system towards MG islanding, two MPPT methods based on the conventional P&O algorithm associated with a DC-DC boost converter were proposed. The first one was implemented with the P&O directly returning the duty-cycle to the converter switching command, being denominated by open-loop; and the second one where the MPPT output voltage signal passes through internal cascaded PI loops before being converted into a duty-cycle signal, being denominated of closed-loop, designed from modifications in the control developed by Mahmood et al. (2015) and Raiker et al. (2021).

The methods have been tested through the evaluation of PV power delivered to the MG based on the performance indexes ripple level, THD, settling time, and steady-state error.

2. MICROGRID DESCRIPTION AND MODELING

The MG configuration studied in this article consists of a PV array, a boost type DC-DC converter, a battery energy storage system (BESS), a bidirectional buck-boost DC-DC (BD), a voltage source inverter (VSI), and LCL type filters feeding resistive loads, as shown in Fig. 1. The islanded mode is switched by a three-phase circuit breaker (CB) connected to the grid (Karimi et al., 2017).

The BESS consists of a set of 47 3.3 V $LiFePO_4$ cells. According to da Silva Junior et al. (2021), the model is based on the interpolation of data obtained in experimental tests carried out by Baronti et al. (2013), which relates the hybridization between its state of charge (SoC) and the open circuit voltage (V_{oc}).

Depending on the MG load scenario and PV state, BESS needs to charge or discharge to maintain power balance. Therefore, a BD is required, being responsible for maintaining the DC-link voltage (V_{dc}) at its setpoint and the SoC within a safe range (de Matos et al., 2015).

The PV source is composed of five 345 W modules, totaling a maximum power of 1,725 W. It was modeled in MATLAB/Simulink considering equivalent circuits and mathematical functions described in Nguyen (2015). It considers several parameters to reach a good real-life approach, such as solar irradiance, temperature, series, parallel resistances, and device saturation.

The project of all PV boost converter elements was implemented according to Erickson (2020), where the representative mathematical steady-state equations are detailed. The electronic switches used, IGBT transistors, and the diodes were considered ideal. Table 1 lists the parameters of the PV array and DC-DC boost converter.

3. CONTROL SYSTEMS

This paper aims to compare PV boost converter MPPT control systems in closed and open loops, while MG operates grid-connected and in islanded modes. It is important to highlight islanding detection is not in the scope of this work. In grid-connected mode, the VSI control system is performed to control DC-link voltage. It was implemented according to Barros and Barros (2017) and is not detailed

Table 1. PV and boost control parameters.

Parameter	Symbol	Value
Maximum Power Voltage	V_{mpp}	37.95 V
Maximum Power Current	I_{mpp}	9.1 A
Solar Array Open Circuit Voltage	V_{oc}	46.3 V
Solar Array Short Circuit Current	I_{sc}	9.6 A
PV Unit power	P_{pv}	1700 W
PV Input Capacitor	C_{pv}	100 μF
PV converter boost inductance	L_{pv}	10.8 μF
Series inductor resistance	R_L	0.1 Ω
Switching frequency	f_c	10 kHz
PV control voltage loop (PI)	K_{p1}, K_{i1}	-0.063, -26
PV control current loop (PI)	K_{p2}, K_{i2}	0.16, 2

here. Note that in this operation mode, the BESS control system is turned off once the main grid compensates for all grid needs.

In islanded mode, the grid-forming control strategy is performed to maintain grid voltage and frequency levels. Droop control provides VSI control support, and the BESS BD control system is turned on to keep a constant DC-link voltage level. All these control strategies are described in the following subsections.

3.1 PV Boost Converter Control

In open-loop control, the conventional MPPT P&O algorithm increases or decreases the duty-cycle value, with a fixed step of 0.0001, which is directly taken to the boost PWM modulator.

In the closed-loop control, the voltage reference (V_{pvref}) from the MPPT is compared to the measured PV output voltage, with a fixed increment of $1V$. The resulting error is taken to a PI control to generate a current reference. This current reference is compared to the current measured in the inductor L_{pv} (i_L) and the error passes through a PI control to generate the duty-cycle of the boost PWM modulator. The control scheme is described in Fig. 2.

To model the controllers, the medium state space model technique has been adopted, relating i_L and v_{pv} to the duty-cycle. Through this technique, developed by Middlebrook and Cuk (1976), it is possible to obtain a model that represents the average variables in the state space, whose result is a valid linear model when working with small perturbations. The converter equations of i_L and v_{pv} for closed S switch are:

$$\frac{di_L}{dt} = -\frac{R_L i_L}{L_{pv}} + \frac{v_{pv}}{L_{pv}}, \tag{1}$$

$$\frac{dv_{pv}}{dt} = -\frac{i_L}{C_{pv}} + \frac{V_{eq} - v_{pv}}{R_{eq} C_{pv}}, \tag{2}$$

where R_{eq} and V_{eq} derives from the linearization of the PV module (Jingxun et al., 2021), R_L is the series resistance of the inductor, and C_{pv} is the capacitance used at the PV output.

From (1) and (2), it is possible to demonstrate the transfer functions $G_{id}(s)$ and $G_{vi}(s)$, which is beyond the scope of this work and were meticulously deduced in Corradini et al. (2015). Therefore, for the control objective, the transfer functions resulting from small disturbance signals

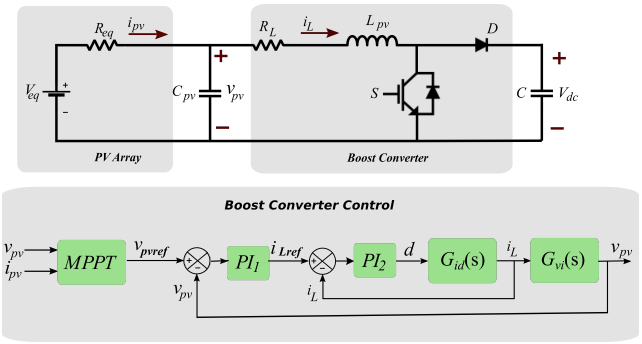

Figure 2. PV Boost Converter Closed-Loop Control.

in i_L and v_{pv} state variables in relation to disturbances in the duty-cycle (d) are described in (3), (4), (5) and (6). The complete $G_{id}(s)$ equation is described in (4) and simplified $G_{id}(s)$ in (5).

$$K = \frac{V_{dc}}{C_{pv} L_{pv} R_{eq}}, \tag{3}$$

$$G_{id}(s) = \frac{K}{\left[s^2 + s\left(\frac{R_L}{L_{pv}} + \frac{1}{C_{pv} R_{eq}}\right) + \frac{R_L}{L_{pv} C_{pv} R_{eq}} + \frac{1}{L_{pv} C_{pv}}\right]}, \tag{4}$$

$$G_{id}(s) = \frac{V_{dc}}{L_{pv} s + R_L}, \tag{5}$$

$$G_{vi}(s) = \frac{-1}{C_{pv} s + \frac{1}{R_{eq}}}. \tag{6}$$

To tune the PI controllers, the known technique of pole placement (Ogata, 2010) was used, taking into account the simplified function of $G_{id}(s)$. Thus, the gains of the controllers can be determined by the function of the converter switching frequency (f_c), resulting in the following voltage loop controller and current loop controller equations:

$$K_{p_1} = -2\pi f_{cv} C_{pv}, \tag{7}$$

$$K_{i_1} = -\frac{2\pi f_{cv}}{R_{eq}}, \tag{8}$$

$$K_{p_2} = \frac{2\pi f_{ci} L_{pv}}{V_{dc}}, \tag{9}$$

$$K_{i_2} = \frac{2\pi f_{ci} R_L}{V_{dc}}. \tag{10}$$

For this paper, the cut-off frequency of the current controller f_{ci} was taken ten times lower than the f_c of the boost, and the cut-off frequency of the voltage controller f_{cv} was taken one hundred times lower than the f_c voltage.

3.2 Droop Control

The VSI uses a droop control in islanding mode which consists in reducing frequency or output voltage when active power or reactive power supplied by the inverter

decreases, respectively. This method was chosen because it allows greater flexibility and reliability in the allocation of physical modules, once it only measures power (Karaki et al., 2019; ZHANG et al., 2018).

The droop control of this paper uses the same strategy described in Vasquez et al. (2013), where an internal proportional-resonant (PR) based on stationary referential works out the control of the sinusoidal reference voltage from the droop to obtain no static error. The simplified diagrams of droop control and PR are shown in Fig. 1.

3.3 Bidirectional buck-boost converter control

The bidirectional control system was implemented with two PI control loops, whose parameters can be seen in Table 2, following the state space model and the entire structure presented in Mahmood et al. (2012), except for the switching between buck and boost modes that were conditioned to work as two unidirectional converters. The simplified diagram of BD control is shown in Fig. 1.

4. SIMULATIONS AND RESULTS

Simulations in MATLAB/Simulink were performed with open-loop and closed-loop MPPTs. The MG control and configuration parameters are listed in Table 2. The tests consist of the analysis of the behavior of the power delivered by the PV, focusing on ripple, THD, settling time, and steady-state error.

In islanded mode, the MG is controlled by droop that allows frequency variation, since the secondary control described in Guerrero et al. (2011) was not implemented. Due to this, to measure the THD, a fast fourier transform (FFT) analysis was performed, identifying the fundamental frequency assumed by the droop in each load situation. This reference value slightly higher or lower than 60Hz was used to correctly generate the THD. The results of this operation are shown in Figs. 8, 7, 9, 10, and summarized in the Table 3.

The tests in islanded mode were performed with purely resistive load Z_L, in four scenarios, $Z_L = 100\ \Omega$, $Z_L = 50\ \Omega$, $Z_L = 24\ \Omega$ and $Z_L = 16.5\ \Omega$.

4.1 Scenario 01 - $Z_L = 100\Omega$

The open-loop PV reached the steady state power of 1,649W in a settling time of 77.5ms. The steady-state error was 76W. It is observed that the power ripple level remains stable in 2.3% of the MPP. THD calculated at 9.37%. This situation is shown in the top graphic in Figs. 3 and 7.

The closed-loop PV reached the steady state power of 1,716W in a settling time of 2ms. The steady-state error was 9W. It is observed that the power ripple level remains stable in 5.8% of the MPP. THD calculated at 9.45%. This situation is shown in the bottom graphic in Figs. 3 and 7.

4.2 Scenario 02 - $Z_L = 50\Omega$

After islanding, the open-loop PV reached the steady state power of 1,649W in a settling time of 42ms. The steady-state error was 76W. It is observed that the power ripple

Table 2. Simulation setup and control parameters.

Parameter	Symbol	Value
DC-Link nominal voltage	V_{cc}	300 V
Grid AC nominal voltage	V_g	127 V_{RMS}
Nominal frequency	f_0	60 Hz
PV Unit power	P_{pv}	1000 W
BESS nominal voltage	V_{BESS}	155 V
BESS capacity	C_{BESS}	20 Ah
BESS converter inductance	L_B	10 mH
BESS-side capacitance	C_{B1}	100 μF
DC-Link-side capacitance	C_{B2}	38 μF
DC-Link capacitances	C_L	500 μF
VSI-side inductance	L_f	500 μH
Grid-side inductance	L_o	500 μH
Filter capacitance	C_f	9 μF
BESS control voltage loop (PI)	K_{bpv}, K_{biv}	0.063, 150
BESS control current loop (PI)	K_{bpi}, K_{bii}	0.2325, 1.57
PR voltage loop	K_{pv}, K_{iv}	500, 500
PR current loop	K_{pi}, K_{ii}	100, 100
Frequency droop coefficient	m	0.005
Voltage droop coefficient	n	1

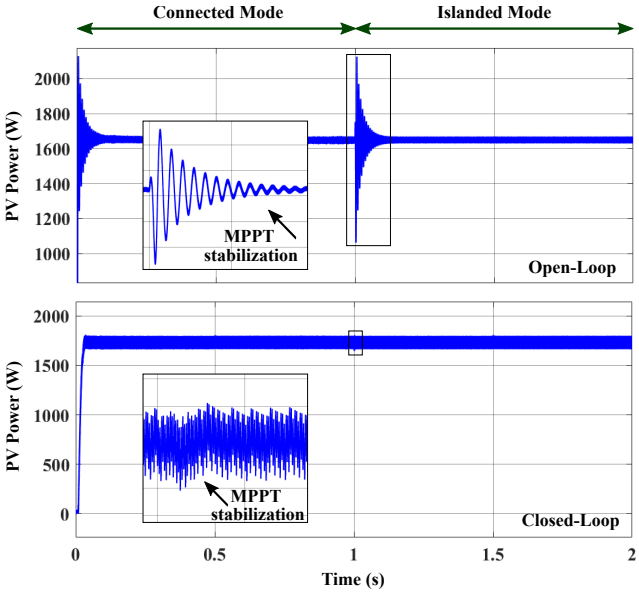

Figure 3. PV power and MPPT stabilization in open and closed-loop, respectively, for $Z_L = 100\ \Omega$.

level remains stable in 2.3% of the MPP. THD calculated at 10.82%. This situation is shown in the top graphic in Figs. 4 and 8.

The closed-loop PV reached the steady state power of 1,716W in a settling time of 9ms. The steady-state error was 9W. It is observed that the power ripple level remains stable in 5.8% of the MPP. THD calculated at 10.61%. This situation is shown in the bottom graphic in Figs. 4 and 8.

4.3 Scenario 03 - $Z_L = 24\Omega$

After islanding, the open-loop PV reached the steady state power of 1,625W in a settling time of 42ms. The steady-state error was 100W. It is observed that the power ripple level becomes quite irregular and shows a greater oscillation reaching 104.62% of the MPP. THD calculated

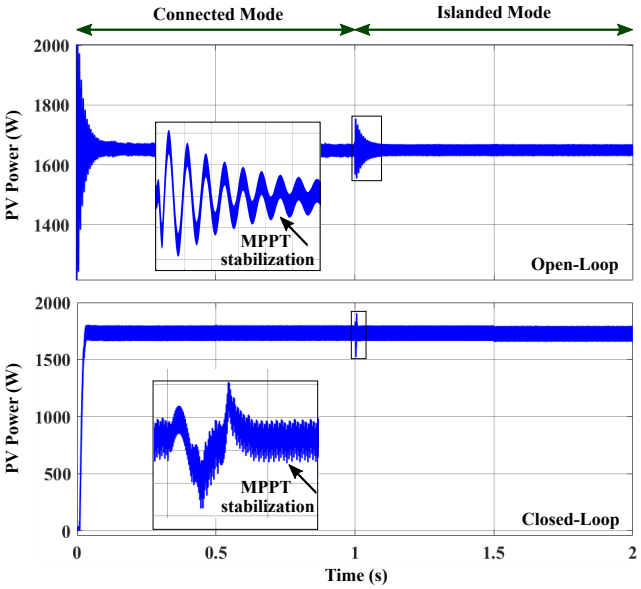

Figure 4. PV power and MPPT stabilization in open and closed-loop, respectively, for $Z_L = 50\ \Omega$.

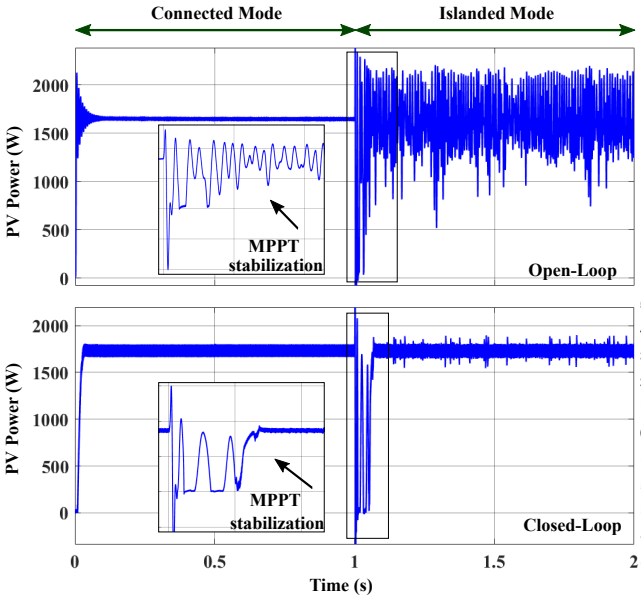

Figure 5. PV power and MPPT stabilization in open and closed-loop, respectively, for $Z_L = 24\ \Omega$.

at 13.43%. This situation is shown in the top graphic in Figs. 5 and 9.

The closed-loop PV reached the steady state power of 1,715W in a settling time of 70ms. The steady-state error was 10W. It is observed that the power ripple level increases but remains stable at 14.6% of the MPP. THD calculated at 13.29%. This situation is shown in the bottom graphic in Figs. 5 and 9.

4.4 Scenario 04 - $Z_L = 16.5\Omega$

The open-loop MPPT reached the steady state power of 1,157W in a settling time of 30ms. The steady-state error was 568W. It is observed that the power ripple level becomes quite irregular and shows a greater oscillation reaching 194.5% of the MPP. THD calculated at 17.27%.

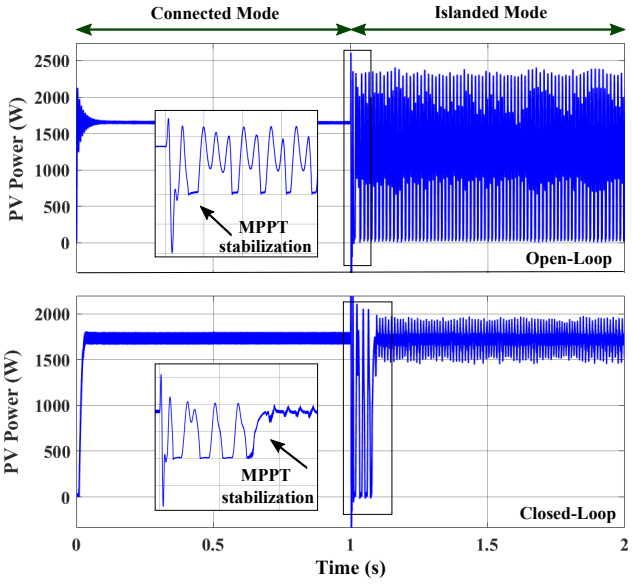

Figure 6. PV power and MPPT stabilization in open and closed-loop, respectively, for $Z_L = 16.5\ \Omega$.

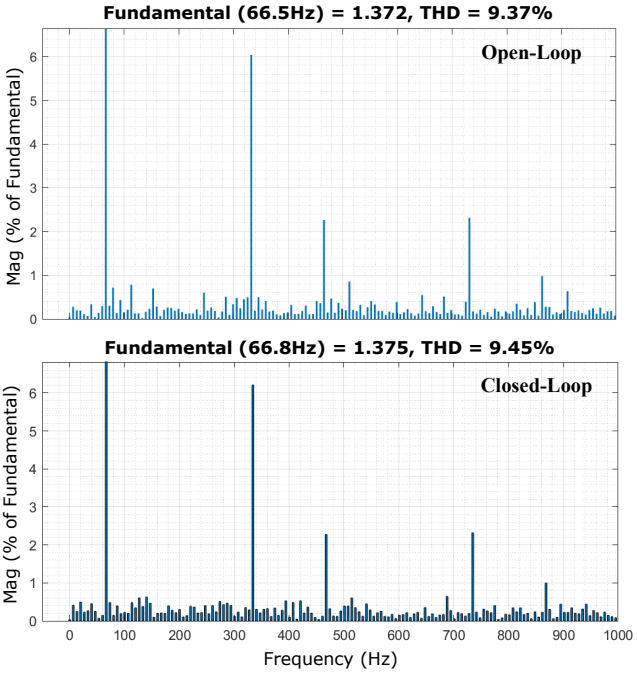

Figure 7. FFT for $Z_L = 100\ \Omega$ in open and closed-loop, respectively.

This situation is shown in the top graphic in Figs. 6 and 10.

The closed-loop PV reached the steady state power of 1706W in a settling time of 95ms. The steady-state error was 19W. It is observed that the power ripple level increases but remains stable in 23.4% of the MPP. THD calculated at 16.88%. This situation is shown in the bottom graphic in Figs. 6 and 10.

CONCLUSION

This paper presents a comparative study of two MPPT methods based on P&O, for photovoltaic generation in a

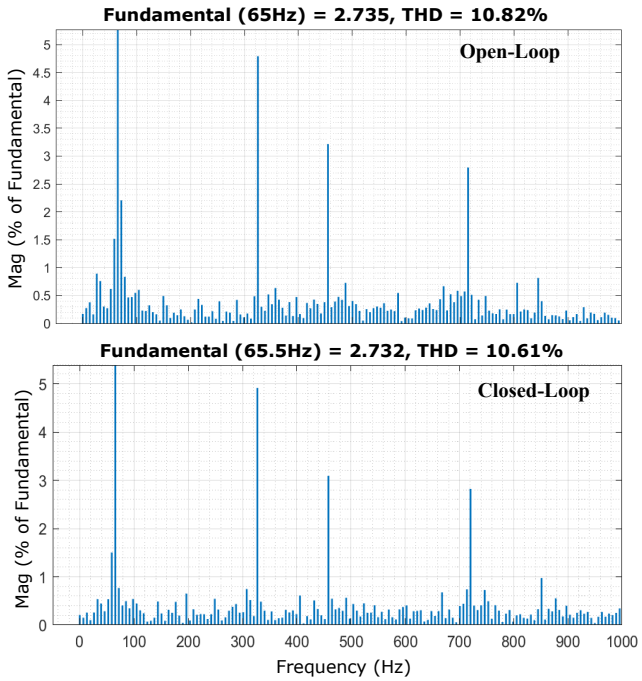

Figure 8. FFT for $Z_L = 50\ \Omega$ in open and closed-loop, respectively.

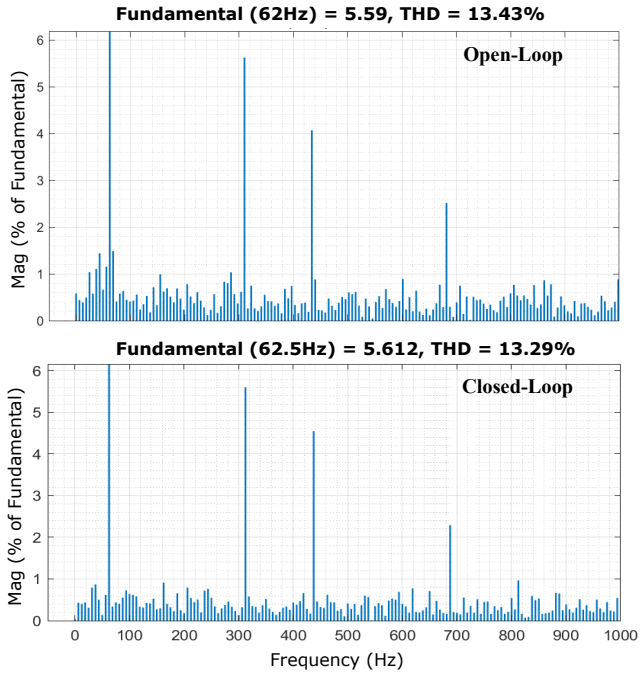

Figure 9. FFT for $Z_L = 24\ \Omega$ in open and closed-loop, respectively.

Table 3. Test Results

	Open-Loop				Closed-Loop			
Load (z_L)	THD	Ripple	Error	S. Time	THD	Ripple	Error	S. Time
100 Ω	9.37%	2.3%	76W	77.5ms	9.45%	5.8%	9W	2ms
50 Ω	10.82%	2.3%	76W	42ms	10.61%	5.8%	9W	9ms
24 Ω	13.43%	104.6%	100W	60ms	13.29%	14.6%	10W	70ms
16.5 Ω	17.27%	194.5%	568W	30ms	16.68%	23.4%	19W	95ms

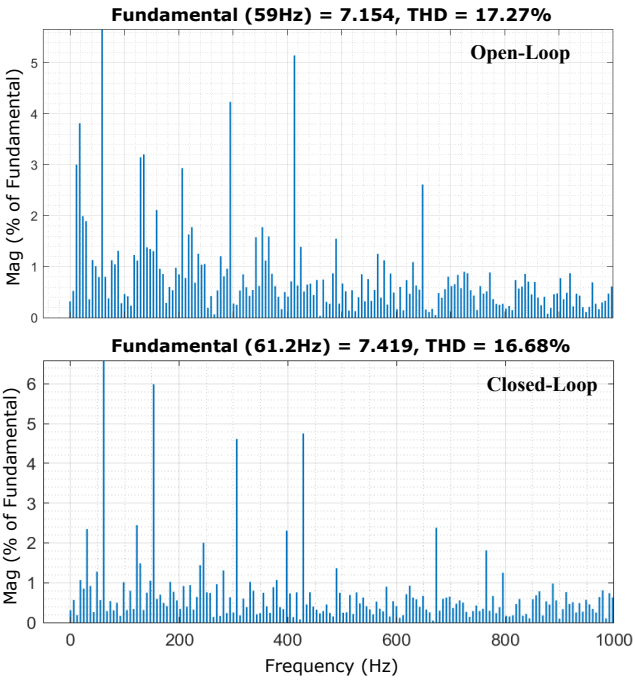

Figure 10. FFT for $Z_L = 16.5\ \Omega$ in open and closed-loop, respectively.

microgrid during islanded operation: open-loop and closed-loop. The closed-loop method has been better since test results show that this controller presented itself as more robust during the islanded mode of the microgrid. The tests focused on photovoltaic power generation ripple level, total harmonic distortion, settling time, and steady-state error, for four different load scenarios. Although the closed-loop has not brought substantial improvement for quality indexes, which are ripple level and total harmonic distortion, dynamic performance indexes have improved, which are settling time and steady-state error, which means a photovoltaic supplying more robust towards islanding guaranteeing a stronger voltage and frequency regulation of the microgrid.

ACKNOWLEDGEMENT

The authors would like to acknowledge the financial support of CAPES. They are also grateful for the institutional support of UFPB, mainly to the Digital System Laboratory (LASID) of Informatics Center (CI), Electrical Engineering Graduation Program (PPGEE), and Graduate Program in Computational Mathematical Modelling (PPGMMC).

REFERENCES

Baronti, F., Zamboni, W., Femia, N., Roncella, R., and Saletti, R. (2013). Experimental analysis of open-circuit voltage hysteresis in lithium-iron-phosphate batteries. In *IECON 2013-39th Annual Conference of the IEEE Industrial Electronics Society*, 6728–6733. IEEE.

Barros, L.S. and Barros, C.M.V. (2017). Modificação no controle do lado da rede de geradores eólicos baseados em pmsg para ampliar a suportabilidade a afundamentos de tensão. *Eletrônica de Potência*, 22(2), 167–178.

Corradini, L., Maksimovic, D., Mattavelli, P., and Zane, R. (2015). *IEEE Press Series on Power Engineering*, a1–a4. doi:10.1002/9781119025498.scard.

da Silva Junior, G.P., Barros, L.S., and Barros, C.M.V. (2021). Synchronverter coupled to a lithium-ion bank for grid frequency and voltage supports and controlled charge-discharge. *Electric Power Systems Research*, 197, 107352.

de Matos, J.G., e Silva, F.S.F., and Ribeiro, L.A.d.S. (2015). Power control in ac isolated microgrids with renewable energy sources and energy storage systems. *IEEE Transactions on Industrial Electronics*, 62(6), 3490–3498. doi:10.1109/TIE.2014.2367463.

Deshpande, A.S. and Patil, S.L. (2016). Performance verification of ripple correlation control for solar pv application. In *2016 7th India International Conference on Power Electronics (IICPE)*, 1–5. doi:10.1109/IICPE.2016.8079510.

Erickson, R. W., M. (2020). *Fundamentals of Power Eletronics*. Springer Nature Switzerland AG. doi: ISBN978-3-030-43881-4.

Esram, T. and Chapman, P. (2007). Comparison of photovoltaic array maximum power point tracking techniques. *Energy Conversion, IEEE Transactions on*, 22, 439 – 449. doi:10.1109/TEC.2006.874230.

Guerrero, J.M., Vasquez, J.C., Matas, J., de Vicuna, L.G., and Castilla, M. (2011). Hierarchical control of droop-controlled ac and dc microgrids—a general approach toward standardization. *IEEE Transactions on Industrial Electronics*, 58(1), 158–172. doi:10.1109/TIE.2010.2066534.

Harrag, A., Messalti, S., and Daili, Y. (2019). Innovative single sensor neural network pv mppt. In *2019 6th International Conference on Control, Decision and Information Technologies (CoDIT)*, 1895–1899. doi:10.1109/CoDIT.2019.8820335.

Jiandong, D., Ma, X., and Tuo, S. (2018). A variable step size p amp;o mppt algorithm for three-phase grid-connected pv systems. In *2018 China International Conference on Electricity Distribution (CICED)*, 1997–2001. doi:10.1109/CICED.2018.8592040.

Jingxun, F., Shaowu, L., Xianping, Z., and Yan, L. (2021). Research on photovoltaic cell models: A review. In *2021 33rd Chinese Control and Decision Conference (CCDC)*, 1006–1011. doi:10.1109/CCDC52312.2021.9602658.

Karaki, A., Begovic, M., Bayhan, S., and Abu-Rub, H. (2019). Frequency and voltage restoration for droop controlled ac microgrids. In *2019 2nd International Conference on Smart Grid and Renewable Energy (SGRE)*, 1–6. doi:10.1109/SGRE46976.2019.9020914.

Karimi, Y., Oraee, H., and Guerrero, J.M. (2017). Decentralized method for load sharing and power management in a hybrid single/three-phase-islanded microgrid consisting of hybrid source pv/battery units. *IEEE Transactions on Power Electronics*, 32(8), 6135–6144. doi:10.1109/TPEL.2016.2620258.

Kim, E., Warner, M., and Bhattacharya, I. (2020). Adaptive step size incremental conductance based maximum power point tracking (mppt). In *2020 47th IEEE Photovoltaic Specialists Conference (PVSC)*, 2335–2339. doi:10.1109/PVSC45281.2020.9300956.

Mahmood, H., Michaelson, D., and Jiang, J. (2012). Control strategy for a standalone pv/battery hybrid system. In *IECON 2012 - 38th Annual Conference on IEEE Industrial Electronics Society*, 3412–3418. doi:10.1109/IECON.2012.6389351.

Mahmood, H., Michaelson, D., and Jiang, J. (2015). Decentralized power management of a pv/battery hybrid unit in a droop-controlled islanded microgrid. *IEEE Transactions on Power Electronics*, 30(12), 7215–7229. doi:10.1109/TPEL.2015.2394351.

Middlebrook, R.D. and Cuk, S. (1976). A general unified approach to modelling switching-converter power stages. In *1976 IEEE Power Electronics Specialists Conference*, 18–34. doi:10.1109/PESC.1976.7072895.

Nguyen, M.P. (2015). Mathematical modeling of photovoltaic cell/module/arrays with tags in matlab/simulink. *Environmental Systems Research*, 4. doi:10.1186/s40068-015-0047-9.

Nguyen, V.T., Hoang, D.H., Nguyen, H.H., Le, K.H., Truong, T.K., and Le, Q.C. (2019). Analysis of uncertainties for the operation and stability of an islanded microgrid. In *2019 International Conference on System Science and Engineering (ICSSE)*, 178–183. doi:10.1109/ICSSE.2019.8823105.

Ogata, K. (2010). *Engenharia de controle moderno*. Pearson Prentice Hall. doi:ISBN978-85-7605-810-6.

Rai, R. and Rahi, O. (2022). Fuzzy logic based control technique using mppt for solar pv system. In *2022 First International Conference on Electrical, Electronics, Information and Communication Technologies (ICEEICT)*, 01–05. doi:10.1109/ICEEICT53079.2022.9768650.

Raiker, G.A., Loganathan, U., and Reddy B., S. (2021). Current control of boost converter for pv interface with momentum-based perturb and observe mppt. *IEEE Transactions on Industry Applications*, 57(4), 4071–4079. doi:10.1109/TIA.2021.3081519.

Vasquez, J.C., Guerrero, J.M., Savaghebi, M., Eloy-Garcia, J., and Teodorescu, R. (2013). Modeling, analysis, and design of stationary-reference-frame droop-controlled parallel three-phase voltage source inverters. *IEEE Transactions on Industrial Electronics*, 60(4), 1271–1280. doi:10.1109/TIE.2012.2194951.

ZHANG, H., GAO, Y., and LU, D. (2018). Micro-grid droop control strategy optimization and simulation. In *2018 China International Conference on Electricity Distribution (CICED)*, 2013–2017. doi:10.1109/CICED.2018.8592279.